IAC–22–C4,8-B4.5A,x72916

End-Of-Life Disposal of Sub-3U CubeSat with a printed thin-film Vacuum Arc Thruster

Kash Saddul[a,*], Alexander Wittig[b], James Saletes[a], Minkwan Kim[b]

[a] *Ph.D. Candidate, Astronautics Research Group*, University of Southampton, United Kingdom
[b] *Associate Professor, Astronautics Research Group*, University of Southampton, United Kingdom
[*] Corresponding author

Abstract

We present the operation of the CubeSat De-orbiting All-Printed Propulsion System (Cube-de-ALPS), a thin-film Vacuum Arc Thruster being developed at the University of Southampton in collaboration with the European Space Agency to provide robust de-orbiting capability to sub-3U CubeSats. It is composed of a flexible substrate on which coplanar arrays of vacuum arc micro-thrusters (micro-VAT) are printed, alongside small supporting electronic subsystems. In particular, we focus on the operations of a Cube-de-ALPS End-Of-Life disposal for an under-actuated spacecraft with uncontrolled spin. In this scenario, a single micro-VAT will ignite every time it points in the direction of the forward velocity vector. Orbital lifetime estimates using simplified dynamics show Cube-de-ALPS can shorten the de-orbiting time from 800 km altitude by up to two orders of magnitude. Due to the design, the micro-thrusters are not aligned with the centre of mass, thus imparting a torque on the spacecraft. We use this in conjunction with a closed-loop thrusting law, to control the spin of the satellite during de-orbiting. These preliminary results are compared to high-fidelity simulations including full six degrees of freedom coupled attitude and orbital dynamics to confirm the viability of the concept.

Keywords: CubeSat, End-Of-Life De-orbiting, Electric Micro-Propulsion, Orbit-Attitude Simulations

1. Introduction

According to the 2020 SpaceWorks forecast, between 1800 and 2500 CubeSats are expected to be launched between 2020 and 2025 [1]. Most of these satellites are for commercial applications, and CubeSats typically use Commercial-Off-The-Shelf components, which leads to a high failure rate, with approximately 25% of all launches ending in a non-responsive spacecraft [2]. If the satellite is unable to perform its mission, it becomes space debris which can cause significant damage to other objects present in Low Earth Orbit (LEO) [3]. To avoid the proliferation of such debris, the Inter-Agency Space Debris Coordination Committee's (IADC) guideline state that a spacecraft in Low Earth Orbit should re-enter the Earth's atmosphere within 25 years past its operational lifetime [4]. The high failure rate and the de-orbiting recommendation lead many CubeSats to be limited to low orbital altitudes to guarantee passive re-entry if the satellite is dead-on-arrival. However, this passive decay also restricts the lifetime of functioning satellites, limiting their operational uptime [5]. For example, at 400 km, a 1U CubeSat is expected to decay naturally within 200 days, while at 600 km, the same satellite is expected to take 20 years to re-enter [6].

To allow operation at higher orbits while maintaining compliance with the IADC guidelines, CubeSats must be equipped with a propulsion system to perform a decommissioning manoeuvre at the end of the mission. However, the vast majority of CubeSats (>95%) are in the Sub-3U ($\leq$3U) range [7], meaning that their mass, volume, and power budgets are severely restricted and do not typically allow for the use of propulsion systems.

Electric Propulsion (EP) systems are particularly interesting for CubeSats, as they typically present high fuel efficiency [8], leading to a smaller amount of fuel required, which could save mass and volume on the spacecraft. However, their implementation is not straightforward, as EP systems tend to come with heavy electronic components and high power requirements [9]. For example, the state-of-the-art for Gridded Ion Thrusters (GITs) [10] on small satellites presents seven GITs, with only one that could be fitted on a 1U, the Ariane Group RIT μX. Indeed, the other GITs presented in the report have a mass greater than 1.33 kg, the maximum weight of a typical 1U CubeSat[11]. The Ariane Group RIT μX is also the least power-consuming of all the GITs shown and typically uses up to 50 W of power. However, 1U CubeSats typically cannot generate more than 2 W of power, and 3U can generally produce up to 10 W, assuming highly efficient solar panels on all six faces [12]. This power constraint means that GITs are unlikely to be used on the smaller range of CubeSats, as they meet neither the mass, volume or power

budget required.

Hall Effect Thrusters (HETs) are an alternative to GITs, which also have more flight heritage on CubeSats [13]. While the average system is lighter than a typical GIT, as there are no grids, the state-of-the-art of HETs for small satellite shows that they tend to be more power intensive than the GITs, with the lowest power requirement being at 53 W [10]. Again, this proves to be unfeasible for CubeSats of the $\leq$3U class.

Electrospray thrusters are a form of EP suitable for the smaller end of CubeSats [14], as some electrospray thrusters have mass, volume, and power requirements compatible with use on Sub-3U CubeSats. For example, the Accion Systems TILE-2 Electrospray thruster weighs 0.45 kg and requires roughly 4 W of power [10]. As it takes only 0.5U in volume, a 3U CubeSat could potentially incorporate it as an actuator. However, these mass and power requirements are still unfeasible for smaller CubeSats. To cater for the smaller range, one could look at the Morpheus Space NanoFEEP thruster, which weighs 0.16 kg, fits physically in a 0.5U space, and requires less than 3 W for operation [15].

Practically, however, none of these options is likely to be used on such limited CubeSats, as attitude control systems are required to operate the thrusters [16]. This requirement for attitude control typically means that the mass, volume, and power budget must also include attitude actuators besides the mission payload.

A lightweight, low-power system is thus required to allow Sub-3U CubeSats to use active de-orbiting methods without significantly sacrificing their mission objectives, which leads to Pulsed Plasma Thrusters (PPTs) and Vacuum Arc Thrusters (VATs) [13, 17]. Both these systems generate an electric arc across the surface of a solid propellant to vaporise and ionise it, with PPTs using Teflon and VATs using metallic propellants. Their simple design and power requirements as low as 0.5 W make them very suitable for smaller CubeSats.

1.1. *CubeSat de-orbiting All-Printed Propulsion System*

As part of ESA's Innovative Propulsion System for CubeSats and MicroSats, a thin-film VAT, named CubeSat de-orbiting All-Printed Propulsion System (Cube-de-ALPS), is being developed at the University of Southampton [18]. It is a fully-printed, flat system that can be placed on the side of a 1U CubeSat and will provide thrust for post-mission disposal. Cube-de-ALPS consists of multiple arrays of micro-Vacuum Arc Thrusters (micro-VATs) that can generate, one at a time, 17.5 μN of thrust at 1.5 W of power. It is arranged in a 10x10 grid to provide 100 micro-VATs, and its theoretical fuel capacity provides it with one year of firing time, by using 100 g of propellant. The developed system is aimed to fit within a 0.2U volume and weighs up to 0.25 kg. We show in Figure 1 a simple estimate of the capabilities of Cube-de-ALPS. In this simulation, a 1U CubeSat equipped with the thruster system fires continuously for one year against the velocity vector, starting from different orbital altitudes. drag and geopotential perturbations, as detailed in Section 2 are included in the simulation. The plot shows the time taken to reach 150 km. Cube-de-ALPS will turn on at the end of the mission

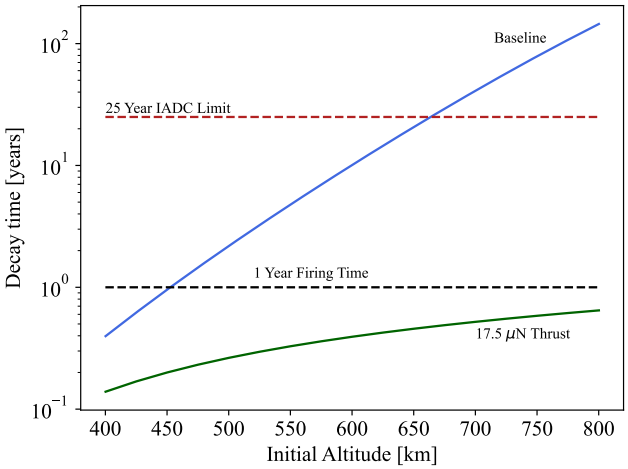

Fig. 1: Decay time with respect to altitude. The plot presents the initial estimates in dark green. The simulation assumes the thrust always acts against the velocity. A baseline, which corresponds to a 1U naturally decaying, is shown in blue.

life of the host CubeSat or shortly after launcher separation if the spacecraft is dead-on-arrival. To ensure de-orbiting, the system must thrust to slow down the orbital velocity of the host CubeSat. Therefore, Cube-de-ALPS must thrust against the velocity direction, which could require an attitude actuator to achieve accurate pointing. However, few Sub-3U CubeSats have active attitude control systems onboard, with most of them having no form of ACS whatsoever [19]. Therefore, throughout this work, the host CubeSat is assumed to be underactuated around all axes. The operational mode of Cube-de-ALPS is, therefore, to ignite a micro-VAT whenever it is pointing partially against the velocity direction, i.e. at any angle that has a component of thrust against the spacecraft's motion.

A distinguishable feature of Cube-de-ALPS is its use of distributed propulsion architecture. Figure 2 shows that similarly to digital propulsion systems, Cube-de-ALPS provides multiple micro-thrusters laid out in a co-planar fashion. Each micro-thruster, also called thruster head or thruster pixel, is an individual micro-VAT capable of delivering thrust. Unlike MEMS-based digital propulsion systems, which have a thruster head radius of less than 0.5 mm [20], the printed VAT has its micro-thrusters at the macroscopic level, with each pixel having a radius of 2.25 mm. Additionally, each printed pixel is re-ignitable,

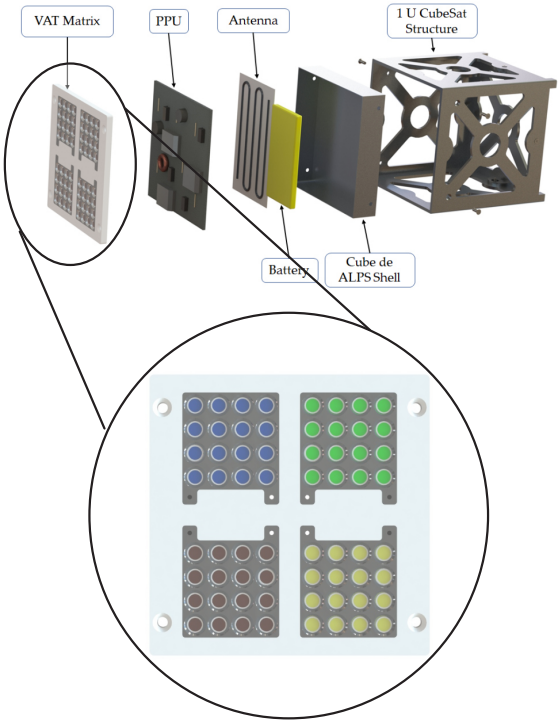

Fig. 2: Representative sketch of Cube-de-ALPS . The division into four quadrants is shown.

contrary to most MEMS-based digital propulsion systems.

The nature of the layout leads most pixels to generate a torque upon firing as they are not aligned with the centre of mass. To counter this effect, Cube-de-ALPS divides its pixels into four individually addressable quadrants. The four zones were chosen to provide essential attitude control while keeping the electronics design simple. Cube-de-ALPS can decide in which quadrant a pixel will ignite, and based on the path of least electrical resistance within the quadrant's circuit, a micro-VAT will ignite. This selection process means Cube-de-ALPS has no control over which exact pixel will ignite. Instead, it can only control in which quadrant a thruster head will turn on.

Every time a given pixel ignites, the thruster head receives a pulsed electrical signal. At each pulse, the micro-VAT will generate a potentially widely different level thrust, according to a thrust distribution function. However, with a high pulse frequency, the average thrust is still closely distributed around the nominal thrust level of each pulse, as per the Central Limit Theorem [21], leading the average thrust to be repeatable.

Table 1 provides a summary of the characteristics of Cube-de-ALPS assumed for the simulations carried out in this work.

Property	Value
Nominal Thrust [μN]	17.5
Pulse standard deviation [%]	10
Pulse frequency [Hz]	100
Number of pixels [-]	100
Grid dimension [-]	10x10
Total burn time [days]	365
Burn time per pixel [days]	3.65

Table 1: Summary of Cube-de-ALPS properties.

2. Simulation Environment

A custom high-fidelity simulation environment was created to assess the effect of Cube-de-ALPS on the de-orbiting time of CubeSats. This section will describe the dynamical models used, the force models included and the reasoning behind their selection.

Perturbing force models are used in combination with the Gaussian form of the Variation of Parameters (Gaussian VOP) to form a simulator capable of propagating the CubeSat [22]. To avoid the singularities at equatorial, polar, and circular orbits, the propagator uses Equinoctial elements [23]. These elements offset the singularity to orbits at 180 degrees of inclination, which are virtually never used. The Equinoctial form of the Gaussian VOP was verified by comparing the results of our simulator to the output of the General Mission Analysis Tool (GMAT).

We included the effect of the thrust of Cube-de-ALPS on the trajectory, as well as the influence of atmospheric drag. The impact of the non-spherical Earth is also modelled, although its effect on the de-orbiting times of CubeSats is minor compared to the thrust and drag. Attitude dynamics are also incorporated into the simulator, to represent the effect of the thruster on the pointing of the satellite.

2.1. *Thrust Modelling*

The thrust can be modelled with

$$\vec{a}_{thrust} = \frac{\vec{T}}{m} \tag{1}$$

where $\vec{T}$ is the thrust vector, and m is the mass of the CubeSat. The simulator assumes the mass of the CubeSat remains constant throughout the simulation, as the fuel only constitutes a small fraction of the total mass. However, the simulation does keep track of fuel consumed by each pixel, to determine when they burn out. Every time a pixel ignites, a thrust value is generated randomly according to a normal distribution, but then remains constant while said pixel fires. Pixels are re-ignitable, so if the same thruster head fires, a new random value is produced. We attach the thrust vector to the location of the pixel which generated

it. The direction of the vector is assumed to be normal to the surface holding the micro-VAT and thus varies with the attitude of the spacecraft.

2.2. *Atmospheric Drag*

The drag is computed using

$$\vec{a}_{Drag} = -\frac{1}{2}\frac{C_D A_{eff}}{m}\rho(h)v_{rel}^2\frac{\vec{v}_{rel}}{\|\vec{v}_{rel}\|} \tag{2}$$

where m is the CubeSat's mass, C_D is the drag coefficient, A_{eff} is the project area, and v_{rel} is the relative velocity between the spacecraft and the rotating atmosphere. The equations are valid in SI units. $\rho(h)$, the atmospheric density, is computed through an interpolation of the Jacchia-77 atmospheric model presented in Frey and Colombo [24]. This model provides an analytical form of the density with respect to altitude and is within 1.5% of the original tabular values. The implementation of the Jacchia-77 interpolation was verified by re-creating the data shown in the original paper by Frey and Colombo [24]. Additionally, the de-orbiting time of a 1U CubeSat in LEO matched the results from GMAT.

2.3. *Geopotential Perturbations*

To model the non-spherical shape of the Earth, a gravity potential is modelled with spherical harmonics. We use the Earth Gravity Model 2008 (EGM08), which uses experimental data from the GRACE and GOCE missions, to determine the coefficients of the harmonic expansion [25, 26, 27]. The EGM08 implementation was verified by comparing the results of the in-house simulator to GMAT. Similarly to the verification of the Equinoctial Gauss Planetary Equations, a 1U CubeSat was placed in a test orbit taken from Curtis [28] and was propagated in both simulators. The difference between the outputs remained below 0.1% for all keplerian elements.

2.4. *Attitude Dynamics*

The attitude dynamics of the CubeSat and its interaction with the orbital motion are modelled using quaternion attitude kinematics [22, 29]. We use a definition of quaternions where the first three elements $q_1\ q_2\ q_3$ correspond to the vector part and q_4 is the scalar part

$$\vec{q} = \begin{pmatrix} q_1 \\ q_2 \\ q_3 \\ q_4 \end{pmatrix} = \begin{pmatrix} \sin\left(\frac{\theta}{2}\right)\vec{e} \\ \\ \cos\left(\frac{\theta}{2}\right) \end{pmatrix} \tag{3}$$

Where the $\vec{e}$ is the principal axis and θ is the Euler angle. This quaternion encodes the rotation from the inertial to the body-fixed frame. The quaternion kinematics are written as

$$\dot{\vec{q}} = \frac{1}{2}\mathbf{\Lambda}\vec{q} \tag{4}$$

$$\mathbf{\Lambda} = \begin{pmatrix} 0 & \omega_z & -\omega_y & \omega_x \\ -\omega_z & 0 & \omega_x & \omega_y \\ \omega_y & -\omega_x & 0 & \omega_z \\ -\omega_x & -\omega_y & -\omega_z & 0 \end{pmatrix} \tag{5}$$

with ω_x, ω_y, ω_z being the components of the angular velocity vector, expressed in the body-fixed frame. The evolution of the angular velocity of an object can be modelled using Euler's equation [30], written as

$$\dot{\vec{\omega}} = \mathbf{I}^{-1}(\vec{\tau}_{total} - \vec{\Omega} \times \mathbf{I}\vec{\omega}) \tag{6}$$

where $\mathbf{I}^{-1}$ is the inverse of the inertia matrix, $\vec{\tau}_{total}$ is the torque applied, $\vec{\Omega} = \vec{\omega}$ is the angular velocity of the CubeSat, and $\dot{\vec{\omega}}$ is the angular acceleration. All parameters from equation (6) are expressed in the body-fixed frame. This differential equation is also where external environmental torques acting on the CubeSat can be added, such as the thruster-induced perturbations.

3. Decommissioning Times Estimates

CubeSats generally do not have actuation systems, and therefore, the assumption that the thruster always points against the velocity vector is unrealistic. Cube-de-ALPS must fire whenever it faces the velocity direction at any angle. An averaging factor is introduced to account for the under-actuated nature of the host satellite. This set of simulations propagates only the orbit and does not include neither the attitude dynamics nor the detailed thrust modelling as described in Section 2. Assuming the CubeSat is spinning randomly, Cube-de-ALPS will, on average, have a component of thrust against the velocity half of the time, i.e. the thruster will point in the correct hemisphere half of the time. Even when it is pointing in the correct hemisphere, the thrust vector is equally likely to point at any angle relative to the velocity direction. We simplify the scenario by assuming all components of thrusts orthogonal to the velocity will eventually cancel out. The thrust along the velocity direction, however, does not cancel out as Cube-de-ALPS never thrusts when facing "backwards". This assumption allows us to compute the average thrust component acting against the velocity for all thrust vector angles in the hemisphere around the velocity vector. This averaging yields an effective thrust four times lower than the nominal value. As we have assumed that we thrust only half of the time, the total time for which we can thrust nominally doubles.

Thus, this set of simulations is similar to the no-attitude set-up, except that the effective thrust is a quarter of the initial value and the firing time doubled to represent the fact that the CubeSat is randomly spinning. Again, the spacecraft was propagated until it reached 150 km. Figure 3 shows the results with the corresponding line labelled "17.5 μN Thrust - averaged". As the thrust is quartered, we notice the CubeSat case takes much longer to de-orbit

than the no-attitude set-up. However, Cube-de-ALPS still provides a significant benefit compared to natural decay. At 800 km, a 1U CubeSat can de-orbit in approximately two years if equipped with the thruster system, even if it is randomly spinning. If Cube-de-ALPS is not present, the same 1U will take over 100 years to decay from that altitude. A dashed line marks the 2-year limit, at which point the thruster runs out of fuel, represented on the curve by an inflection point.

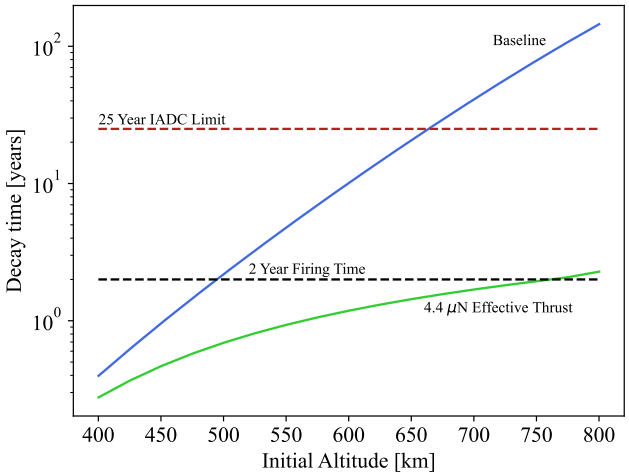

Fig. 3: Decay time with respect to altitude. The plot presents the thrust-averaged estimates in bright green. A baseline, which corresponds to a 1U naturally decaying, is shown in blue.

4. Results

This section details the high-fidelity results of the de-orbiting simulations. We first focus on the implications of the thruster architecture on the attitude of the CubeSat and therefore ignore any orbital modelling. We then combine the orbital and attitude dynamics to confirm the viability of the system.

4.1. *Operation of Cube-de-ALPS*

The flat architecture of Cube-de-ALPS means its micro-thrusters are not centred above the centre of mass of the CubeSat. This misalignment leads a torque to be generated upon firing, inducing a rotation. If not mitigated, the angular velocity can build up to a point where the centrifugal force threatens the structural integrity of the CubeSat. This section presents the problem of controlling this angular velocity with Cube-de-ALPS on a 1U, and offers a practical solution. We simulated a realistic satellite by modelling the SLUCUBE CubeSat [31], a 1U system. The inertia matrix is given, in kg m^2, as

$$\mathbf{I} = \begin{pmatrix} 0.00182 & 0 & 0 \\ 0 & 0.00185 & 0 \\ 0 & 0 & 0.00220 \end{pmatrix} \tag{7}$$

and the CubeSat is assumed to have only Cube-de-ALPS as an actuation system. The objective of the thruster is to provide de-orbiting capacity and to limit the angular velocity build-up. From the literature, an angular velocity of less than one rotation per minute is typically deemed acceptable for most CubeSat missions [32, 33, 34], and therefore, the objective is to maintain the angular rate below 6 $^{\text{deg}}/_{\text{s}}$.

As we ignore the orbital propagation, the system can fire without regard for where it is pointing. Cube-de-ALPS is equipped with a thrust law. Based on the angle of the thruster relative to the velocity direction, the control law will determine whether it should fire or not. We present an uncontrolled thrust law, which does not account for the quadrants present on the system, and a closed-loop thrusting law which regulates the angular velocity. The latter develops the uncontrolled thrust law to also take the angular velocity vector of the satellite as an input, and outputs in which quadrant a pixel should be ignited.

4.2. *Uncontrolled Thrust Law*

In this version, the quadrant division is removed (i.e., only one zone contains all the thruster heads), so a pixel will ignite entirely randomly. It is also assumed that when a pixel ignites, it will continuously fire until it burns out. As the fuel is uniformly distributed across the pixels, the firing time per pixel is

$$t_{burntime} = \frac{365 \text{ days}}{n_{pixels}} = 3.65 \text{ days} \tag{8}$$

where n_{pixels} is the number of pixels on the grid. The result in Figure 4 shows the results of firing Cube-de-ALPS in an uncontrolled manner. The plot shows 40 runs, with 39 plotted in grey and one plotted in orange, as an example case. Already, within the first 5 minutes of firing, we notice the angular velocity has crossed our upper limit of 6 $^{\text{deg}}/_{\text{s}}$ (one rotation per minute). This quick build-up of rotational speed clearly shows the problem linked to naively using Cube-de-ALPS. From Figure 5 we observe that the velocity behaviour changes slope after 3.65 days, which corresponds to the pixel firing time. The plot also indicates that the angular velocity can grow to unreasonable amounts when using a naive approach.

Two main points can be concluded regarding the naive approach's rise in the angular velocity. Firstly, the long, continuous firing of a pixel quickly leads the angular velocity to grow over our acceptable limit of 6 $^{\text{deg}}/_{\text{s}}$. Secondly, due to the random nature of the pixel selection, thruster heads increasing the angular velocity are sometimes ignited consecutively. This successive firing means that two (or more) pixels in a row will accumulate their effect. This issue is independent of the firing time, and even if the pixels fired for a short amount of time, there

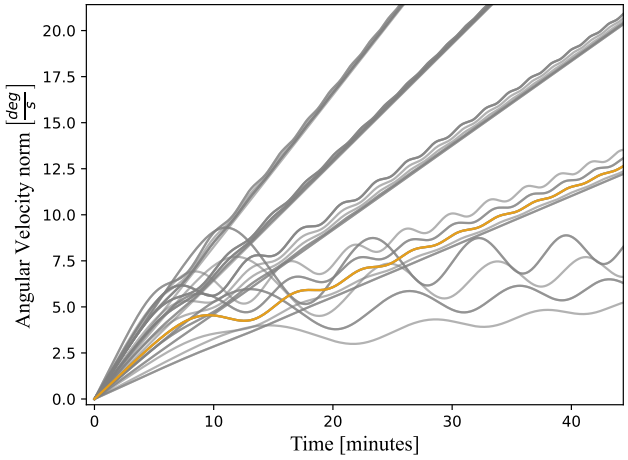

Fig. 4: Evolution of the angular velocity in a naive operation. The figure focuses on the first few minutes of operation. The non-linear motion present is due to the non-ideal inertia matrix of the SLUCUBE satellite. 40 runs are presented, with one highlighted in orange as an example.

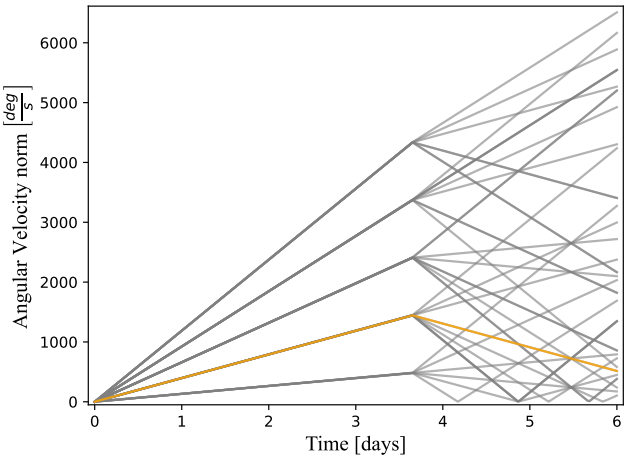

Fig. 5: Evolution of the Angular Velocity in a naive operation, for 6 days. 40 runs are presented, with one highlighted in orange as an example.

would be a possibility that multiple consecutive thruster heads create torques that provide angular acceleration.

4.3. *Closed-Loop Thrusting Law*

By dividing the Cube-de-ALPS into four quadrants, and measuring the angular velocity, we can avoid the issue previously described. In this approach, Cube-de-ALPS requires knowledge of the angular velocity vector to determine which quadrant should be selected. Once the decision is made, a pixel will ignite at random within the chosen quadrant and fire for t_{firing}, the firing time of a pixel. Here, we introduce the distinction between "burn time" and "firing" time. The burn time $t_{burntime}$ refers to the total time a pixel can thrust for and is dependent only on the fuel capacity and distribution. The firing time t_{firing} corresponds to the time for which a pixel will ignite before another micro-thruster fires, which is a parameter of the thrusting law.

The closed-loop thrusting law assesses the angle relative to the orbital velocity and the angular velocity vector on a discrete basis. After a pixel continuously fires for t_{firing}, Cube-de-ALPS re-assesses the required parameters and determines which quadrant should ignite. Therefore, the time between each assessment of the thrusting law, called Quadrant Ignition Time (QIT), is also equal to the pixel firing time, so that $t_{firing} = t_{QIT}$.

To minimise the angular velocity of the CubeSat, the thrusting law always attempts to fire a quadrant that should lead to the minimum final angular velocity. We estimate the effect of each quadrant by assuming a pixel situated at the centre of each zone will fire at the nominal thrust value, and using

$$\vec{\omega}_{est.} = \vec{\omega}_0 + \mathbf{I}^{-1}\vec{\tau}_{centre,i}t_{QIT} \tag{9}$$

where t_{QIT} is the QIT in seconds, $\vec{\tau}_{centre,i}$ is the torque produced from firing a pixel at the centre of the quadrant i at the nominal thrust value (in Nm), and $\mathbf{I}$ is the inertia matrix of the satellite. $\vec{\omega}_{est.}$ and $\vec{\omega}_0$ are the estimated and initial angular velocity vectors. All parameters are expressed in the body-fixed frame.

In this estimation, we assume the angular velocity remains low enough so that the product of the components of $\vec{\omega}_0$ can be ignored. In other words, we ignore the cross product in Equation (6). The consequence of this assumption is that we overlook the cross-coupling of angular velocity due to unequal mass distribution. However, this allows for analytical computation of this estimation at the cost of higher accuracy in the prediction.

Figure 6 shows an example evolution of the angular velocity of a 1U CubeSat equipped with Cube-de-ALPS when the closed-loop thrusting law is applied. This example uses a QIT of 100 seconds. The plot presents 40 runs, with 39 in grey and 1 in orange. As opposed to Figure 5, using this thrusting law allows the angular velocity to be controlled. Indeed, the rotational rate remains mostly below 3 $^{\text{deg}}/_{\text{s}}$, throughout most of the thrusting time. At the very end, we notice a spike in the angular velocity. While it varies on a case-by-case basis, the velocity spike generally increases the rotational rate significantly (sometimes nearly a tenfold increase) and happens around 5 to 10 days before Cube-de-ALPS runs out of fuel.

The fuel consumption pattern of the thruster explains the presence of this spike. Due to the symmetric architecture of Cube-de-ALPS , every pixel has a "conjugate" placed symmetrically opposite on the face. If a pixel and its symmetrically opposite micro-VAT produce the same

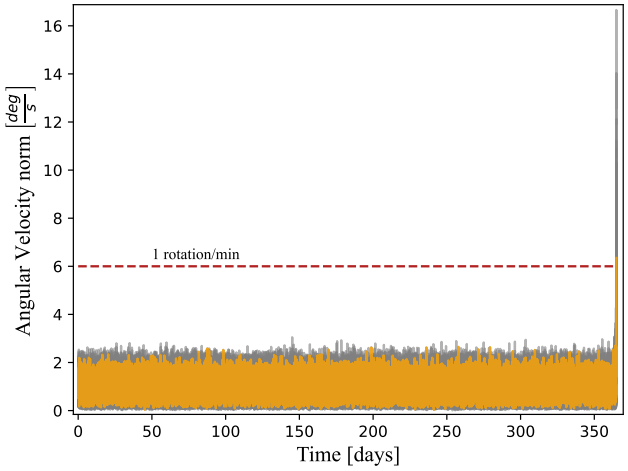

Fig. 6: Evolution of the angular velocity norm when Cube-de-ALPS uses the thrusting law, with a QIT of 100 seconds. 39 runs are in grey, and one is presented in orange.

thrust, their torques should cancel. Ideally, this pair of pixels should ignite successively to ensure that the motion is always balanced out, but the random nature of the pixel selection rarely allows for this. Instead, multiple pixels igniting sequentially often do not form a conjugate pair. Towards the end of the manoeuvre, multiple pixels remain on Cube-de-ALPS , whose torques do not cancel out but instead accumulate to increase the angular velocity. Figure 7 shows an example of the percentage of the total remaining fuel in each quadrant after 355 days of firing (97.2% of the burn time) with a QIT of 100 seconds. There is a clear

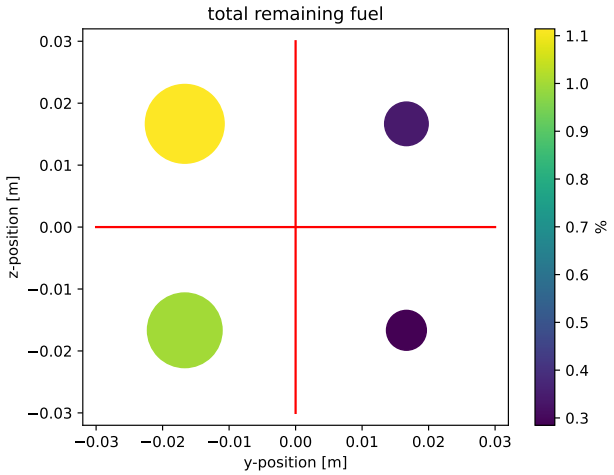

Fig. 7: Example remaining fuel in each quadrant after 355 days of firing Cube-de-ALPS . The thrusting law uses a QIT of 100 seconds. This fuel discrepancy leads to velocity spikes.

difference between each zone, demonstrating that random firing can increase the angular velocity at the end of the manoeuvre.

We consider two practical approaches as the issue happens towards the end of the manoeuvre. In the first approach, as Cube-de-ALPS performs a de-orbiting manoeuvre, it is safe to assume that the spacecraft will be inoperative after the thruster system has burned out, as it will be on a re-entry trajectory. Thus, the rotational rate of the spacecraft does not matter, and this velocity spike does not need any correcting. However, a spacecraft operator could determine that the angular velocity rise is unacceptable. In the second approach, the operation of Cube-de-ALPS stops before it experiences the velocity spike. The angular velocity rise happens up to ten days before the thruster runs out of fuel, at which point the thruster has delivered over 97% of its impulse. As a result, the decay times are not significantly affected by this operational approach.

The intensity of the velocity spike, like the performance of the thrusting law, depends on the QIT chosen. We briefly summarise here the effect of the QIT on the overall performance of the Cube-de-ALPS thrusting law. Figure 8 shows the effect of various QIT values on the average velocity, standard deviation, and the maximum velocity detected. These statistical values were gathered over 40 runs for each QIT. As expected, as the QIT goes down, the average angular velocity becomes smaller, and so does its standard deviation. This trend implies that the performance of the thrusting law is not only better but also more repeatable at lower QITs. As Cube-de-ALPS fires a pixel for less time and switches thruster heads more often, the torque produced is routinely adjusted to minimise the angular velocity, controlling the angular rate. The clear trend suggests that an operator should always choose a low QIT. The only drawback of a short QIT is the reduced time available to perform any of the computations required for the thrusting law. Additionally, using the electronics and onboard computer more often leads to increased power consumption. While it is doubtful that this shortcoming will be of significant importance, a QIT of 100 seconds is chosen to provide both angular velocity control and feasibility with regard to computation time and power requirements.

The definition of the thrusting law has now introduced an additional requirement on Cube-de-ALPS . The system needs to measure the angular velocity of the host CubeSat periodically. It is essential to highlight here that the thrusting law does not concern itself with the pointing of the spacecraft and solely focuses on stabilising the angular velocity. Hence, full attitude knowledge is not required. Only the angular velocity vector is needed, which gyroscopes can provide. These sensors are small and light enough to integrate even with 1U CubeSats easily.

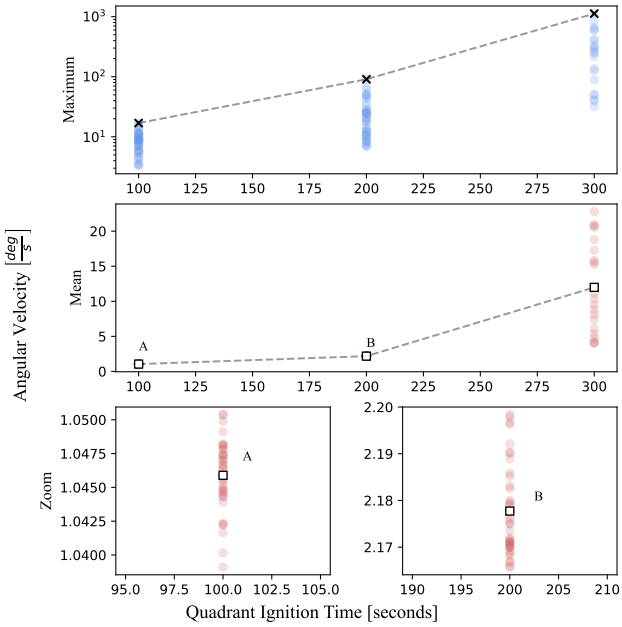

Fig. 8: Effect of Quadrant Ignition Time (QIT) on the angular velocity of a 1U CubeSat. For each QIT, 40 runs were executed. The maximum angular velocity of each run is shown by the blue circles (top), while the black crosses mark the maximum over the 40 runs. The white squares (middle) represent the mean angular velocity over 40 runs, with the average of each individual simulation shown by the red circle. For the QITs of 100 and 200 seconds (points "A" and "B" respectively), the dispersion of the red circles is so small that it is invisible in the middle plot. Therefore, two subplots (bottom) focus on the respective points.

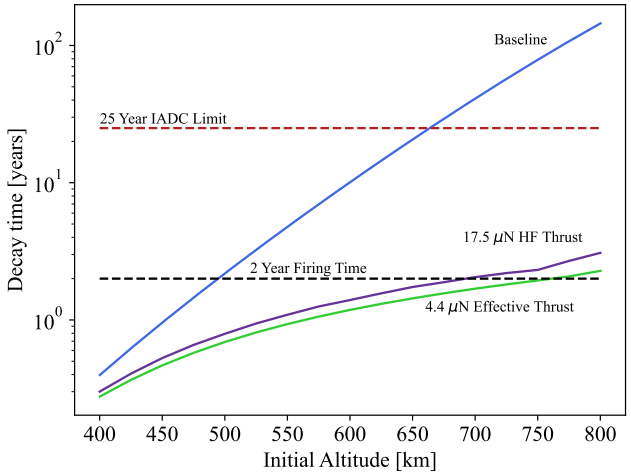

Fig. 9: Decay time with respect to altitude. The plot presents the thrust-averaged estimates in bright green while the High-Fidelity results are shown in purple. A baseline, which corresponds to a 1U naturally decaying, is shown in blue.

4.4. *High-Fidelity Decommissioning Times*

The previous subsection demonstrated that a simple thrusting law, combined with an instrument to detect the angular and orbital velocity, can mitigate the excessive rotational motion induced by Cube-de-ALPS . In this subsection, the focus shifts to the de-orbiting performance of the thruster system. We simulate the decay times of a 1U CubeSat equipped with Cube-de-ALPS at various initial altitudes and present the results of using the complete simulation environment described in Section 2, propagating both attitude and orbital dynamics.

In this set-up, the 1U CubeSat is given an initial rotation of 15 $^{deg}/_{s}$ around each axis, to represent a randomly tumbling spacecraft. The total angular velocity is therefore of 25 $^{deg}/_{s}$. Cube-de-ALPS will fire whenever it faces somewhat in the velocity direction, so the angle at which the thrust acts is not pre-determined. Because of this, the thrust produced by the system is not averaged and is 17.5 μN. Cube-de-ALPS also keeps track of the fuel used, so no assumptions over the firing time are required. The thrust produced will affect the rotational state and the orbital trajectory. Cube-de-ALPS will use the closed-loop thrusting law detailed in 4.3.

Figure 9 shows the results, where the label "17.5 μN HF Thrust" indicates the corresponding line. We notice the High-Fidelity results closely match the averaged thrust method. They both represented the same operational principles, which provided confidence in the outputs. The inflection point, corresponding to Cube-de-ALPS running out of fuel, also happens around the 2-year mark, which validates the assumption that the fuel takes nominally two years to be fully consumed. With the CubeSat initially spinning at 25 $^{deg}/_{s}$, the thrusting law managed to bring the rotational speed down to below 3 $^{deg}/_{s}$ on average throughout the manoeuvre in less than 24 hours, as shown in Figure 10. Figure 11 shows the angular velocity behaviour throughout the simulation time and demonstrates Cube-de-ALPS 's capacity for recovering a 1U spinning out of control. It is helpful to remember that we show the angular velocity profiles of a 1U CubeSat starting at different initial altitudes. Therefore, the decay time, and thus the simulation time, will vary based on the CubeSat's initial orbit. The plot presents velocity spikes, which correspond to the few cases that have fired until Cube-de-ALPS runs out of fuel. As seen in Figure 11, most cases reach the stop condition before the fuel runs out, meaning they will not experience a velocity spike. To conclude this section, we briefly compare the computational cost of the high-fidelity simulations to the thrust-averaged initial estimates. The difference between the two is the method used to account for the attitude. The complete modelling of the attitude is a computationally expensive task, as the inertia matrix

ID	Label	Orbital Perturbations	Attitude included	Thrust direction
No-Attitude	17.5 μN Thrust	Drag & EGM08	No	Against velocity
Thrust-Averaged	4.4 μN Effective Thrust	Drag & EGM08	Analytically	Against velocity
High-Fidelity	17.5 μN HF Thrust	Drag & EGM08	Numerically	Propagated

Table 2: Summary of the different simulations performed.

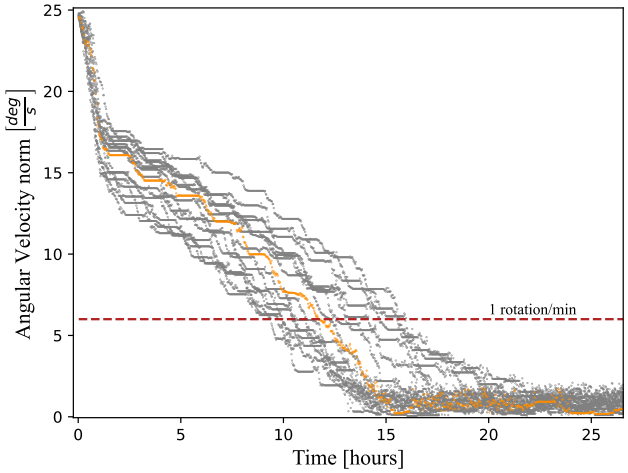

Fig. 10: Angular velocity of the 1U CubeSat during the High-Fidelity simulations. From an initial spin of 25 $^{deg}/_{s}$, Cube-de-ALPS recovers attitude control within a day. One line is plotted in orange as an example to highlight the profile of the angular velocity at the start of the simulation.

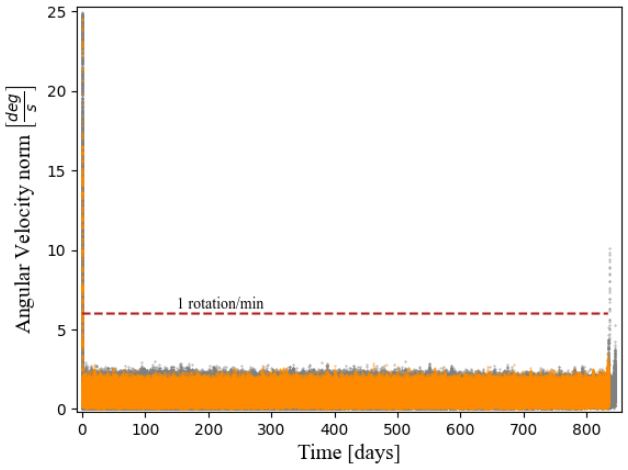

Fig. 11: Angular velocity of a 1U CubeSat throughout the High-Fidelity simulations. Different runs started at different altitudes, hence they do not have matching simulation times. The orange line shows an example profile for a given simulation.

of the 1U CubeSat is realistic. Therefore, the initial estimates run much faster as they ignore the propagation of the spacecraft's orientation. As an example, the results for the averaged thrust on Figure 9 took about 3 hours to run on the author's laptop, while the High-Fidelity simulations required around two weeks on a High-Performance Computer to finish. Given the relative proximity of the averaged results to the High-Fidelity output, it is likely that using the analytical averaging approach will be sufficient for de-orbiting time estimates.

5. Conclusion

In this work, we have introduced Cube-de-ALPS , a printed, flat thruster designed to be integrated on CubeSats as small as 1Us. The thruster system is a failsafe capable of delivering thrust to provide extended de-orbiting capacity to nanosatellites that would otherwise have to rely on the atmospheric drag to re-enter within 25 years, thus restricting their operation to low altitudes. Preliminary estimates have shown that the thruster system has the potential to significantly reduce the decay time of its host CubeSat to the point where even at 800 km, the spacecraft would be IADC compliant. The impact of the under-actuated nature of the host satellite was accounted for analytically, and while the rotation worsened the results, the CubeSats still re-entered the atmosphere within the 25 years recommended by the IADC. In the high-fidelity simulations, the impact of the thruster on the attitude was modelled. The unconventional architecture of Cube-de-ALPS can induce undesirable torques, which we mitigated by implementing a simple thrusting law. This showed that the angular velocity of the host CubeSat could be controlled and lowered to below 3 $^{deg}/_{s}$ for most of the firing time. The focus was then shifted to the de-orbiting performance of Cube-de-ALPS, having solved the issue tied to the angular velocity. We compared the initial estimates to a high-fidelity model of the thruster, operated to de-orbit a 1U CubeSat. Additionally, the high-fidelity results showed that the thrusting law controlled the angular velocity throughout the de-orbiting manoeuvre. Despite starting with an initial angular velocity of 25 $^{deg}/_{s}$, Cube-de-ALPS recovered the spin of the host CubeSat within 24 hours.

Acknowledgments

This work was supported by the European Space Agency under contract number 4000132060/20/NL/RA.

The authors acknowledge the use of the IRIDIS High-Performance Computing Facility and associated support services at the University of Southampton, in the completion of this work.

References

[1] SpaceWorks. Nano/Microsatellite Market Forecast 10th Edition. 2020.

[2] Thyrso Villela, Cesar A Costa, Alessandra M Brandão, Fernando T Bueno, and Rodrigo Leonardi. Towards the thousandth CubeSat: A statistical overview. *Int. J. Aerosp. Eng.*, 2019, 2019. ISSN 16875974. doi: 10.1155/2019/5063145.

[3] Hugh G Lewis, Benjamin S Schwarz, Simon G George, and Hedley Stokes. An assessment of CubeSat collision risk. Technical report.

[4] NASA. Process for Limiting Orbital Debris -NASA-STD-8719.14B. Technical report.

[5] Daniel L Oltrogge and Kyle Leveque. An Evaluation of CubeSat Orbital Decay. *25th Annu. AIAA/USU Conf. Small Satell.*, (August 2011):0–12, 2011.

[6] Li Qiao, Chris Rizos, and Andrew G Ag Dempster. Analysis and Comparison of CubeSat Lifetime. *Proc. 12th Aust. Sp. Dev. Conf.*, pages 8–10, 2013.

[7] N M Suhadis. *Statistical overview of cubesat mission*. Number March 2003. Springer Singapore, 2020. ISBN 9789811547553. doi: 10.1007/978-981-15-4756-0_50.

[8] Roger Birkeland. CubeSat propulsion: Expanding the affordable space platform. (January), 2018.

[9] Jennifer Hudson, Sara Spangelo, Andrew Hine, Daniel Kolosa, and Kristina Lemmer. Mission analysis for CubeSats with micropropulsion. *J. Spacecr. Rockets*, 53(5):836–846, 2016. ISSN 15336794. doi: 10.2514/1.A33564.

[10] Small Spacecraft Technology. State of the Art report. Technical report, 2021.

[11] R Munakata. Cubesat design specification rev. 13. *CubeSat Program, Calif. Polytech. State ...*, 8651:22, 2009.

[12] Craig Clark. Clark SSC10-III-5 Huge Power Demand...Itsy-Bitsy Satellite: Solving the CubeSat Power Paradox. Technical report.

[13] Akshay Reddy Tummala and Atri Dutta. An overview of Cube-Satellite propulsion technologies and trends. *Aerospace*, 4(4):1–30, 2017. ISSN 22264310. doi: 10.3390/aerospace4040058.

[14] Igor Levchenko, Kateryna Bazaka, Yongjie Ding, Yevgeny Raitses, Stéphane Mazouffre, Torsten Henning, Peter J Klar, Shunjiro Shinohara, Jochen Schein, Laurent Garrigues, Minkwan Kim, Dan Lev, Francesco Taccogna, Rod W Boswell, Christine Charles, Hiroyuki Koizumi, Yan Shen, Carsten Scharlemann, Michael Keidar, and Shuyan Xu. Space micropropulsion systems for Cubesats and small satellites: From proximate targets to furthermost frontiers. *Appl. Phys. Rev.*, 5(1), 2018. ISSN 19319401. doi: 10.1063/1.5007734.

[15] Morpheus Space Inc. https://www.morpheus-space.com/products/nanofeep, 2021.

[16] Gary Quinsac, Boris Segret, Christophe Koppel, and Benoît Mosser. Attitude control: A key factor during the design of low-thrust propulsion for CubeSats. *Acta Astronautica*, 176:40–51, 11 2020. ISSN 00945765. doi: 10.1016/j.actaastro.2020.03.053.

[17] Kristina Lemmer. Propulsion for CubeSats. *Acta Astronaut.*, 134(January):231–243, 2017. ISSN 00945765. doi: 10.1016/j.actaastro.2017.01.048.

[18] James Saletes, Minkwan Kim, Kash Saddul, Alexander Wittig, Karim Honda, and Pekka Katila. Development of a novel CubeSat de-orbiting all printed propulsion system. Technical report.

[19] Halis C Polat, Josep Virgili-Llop, and Marcello Romano. Survey, Statistical Analysis and Classification of Launched CubeSat Missions with Emphasis on the Attitude Control Method. *JoSS*, 5(3):513–530, 2016.

[20] David H Lewis, Siegfried W Janson, Ronald B Cohen, and Erik K Antonsson. Digital micropropulsion. Technical report, 2000.

[21] Peck Roxy, Olsen Chris, and Devore Jay. Introduction to Statistics and Data Analysis. Technical report.

[22] D A Vallado. *Fundamentals of Astrodynamics and Applications*. Microcosm Press, 2013.

[23] M J H Walker and Joyce Owens. A set of modified equinoctial orbit elements. Technical report.

[24] Stefan Frey, Camilla Colombo, and Stijn Lemmens. Extension of the King-Hele orbit contraction method for accurate, semi-analytical propagation of non-circular orbits. *Adv. Sp. Res.*, 64(1):1–17, 2019. ISSN 18791948. doi: 10.1016/j.asr.2019.03.016.

[25] Nikolaos K Pavlis, Simon A Holmes, Steve C Kenyon, and John K Factor. The development and evaluation of the Earth Gravitational Model

2008 (EGM2008). *J. Geophys. Res. Solid Earth*, 117(4):1–38, 2012. ISSN 21699356. doi: 10.1029/2011JB008916.

[26] Weiyong Yi and Reiner Rummel. A comparison of GOCE gravitational models with EGM2008. *J. Geodyn.*, 73:14–22, 2014. ISSN 02643707. doi: 10.1016/j.jog.2013.10.004.

[27] Thomas D Papanikolaou and Dimitrios Tsoulis. Assessment of earth gravity field models in the medium to high frequency spectrum based on GRACE and GOCE dynamic orbit analysis. *Geosci.*, 8(12):1–18, 2018. ISSN 20763263. doi: 10.3390/geosciences8120441.

[28] H Curtis. *Orbital Mechanics for Engineering students*. Elsevier, 2005.

[29] F Landis Markley and John L Crassidis. *Fundamentals of Spacecraft Attitude Determination and Control*.

[30] Y. Yang. Spacecraft attitude determination and control: Quaternion based method. *Annual Reviews in Control*, 36(2):198–219, 2012. ISSN 13675788. doi: 10.1016/j.arcontrol.2012.09.003.

[31] Sanjay Jayaram and Darren Pais. Model-based Simulation of Passive Attitude Control of SLUCUBE-2 Using Nonlinear Hysteresis and Geomagnetic Models. *Int. J. Aerosp. Sci.*, 1(4):77–84, 2012. doi: 10.5923/j.aerospace.20120104.04.

[32] Samir A Rawashdeh and James E Lumpp. Nano-Satellite Passive Attitude Stabilization Systems Design by Orbital Environment Modeling and Simulation. Technical report, 2010.

[33] David T Gerhardt and Scott E Palo. Passive Magnetic Attitude Control for CubeSat Spacecraft. *Small Satell. Conf.*, page 10, 2010.

[34] Stephanie Jarmak, Julie Brisset, Joshua Colwell, Adrienne Dove, Douglas Maukonen, Samir A. Rawashdeh, Jürgen Blum, and Larry Roe. CubeSat Particle Aggregation Collision Experiment (Q-PACE): Design of a 3U CubeSat mission to investigate planetesimal formation. *Acta Astronautica*, 155:131–142, 2 2019. ISSN 00945765. doi: 10.1016/j.actaastro.2018.11.029.